JMEPEG (2020) 29:7891–7898
https://doi.org/10.1007/s11665-020-05314-7

1059-9495/$19.00

Gel-Casting Prepared Porous Si_3N_4 Ceramics with Different Contents of Y_2O_3 and Al_2O_3 Additives

Chunrong Zou, Shaojun Guo, Xiaosong Zhou, Song Li, Chunlei Yan, and Tongsheng Shen

Submitted: 24 August 2020 / Revised: 7 October 2020 / Accepted: 13 October 2020 / Published online: 18 November 2020

Porous Si_3N_4 ceramics were prepared via a controlled gel-casting process followed by gas pressure sintering with 8 wt.% Y_2O_3 and Al_2O_3 additives. The gel-casting parameters including slurry pH value, AM: MBAM ratio, degassing procedure, drying condition and decarbonize process were optimized, and the effects of different Y_2O_3: Al_2O_3 ratios on the microstructure and properties of the Si_3N_4 ceramics were investigated. With an optimized gel-casting process, a high solid loading of 46.5 vol.% was achieved, and as the Y_2O_3 content decreased from 6 to 1 wt.%, the porosity of Si_3N_4 ceramics declined from 36.3 to 27.5% while the β-Si_3N_4 phase content reduced from 38.9 to 15.0%. The bending strength and elastic modulus of the ceramics varied with different Y_2O_3: Al_2O_3 ratios and were influenced by the porosity as well as the tailored interlocking structure of elongated β-Si_3N_4 grains. The Si_3N_4 ceramics also exhibited low and stable dielectric constants.

Keywords dielectric properties, gel-casting, mechanical properties, microstructure, Si_3N_4 ceramics

1. Introduction

Silicon nitride (Si_3N_4) ceramic has been widely used as structural and functional materials because of its excellent mechanical, thermal and electrical properties. With respect to wave-transparent applications, Si_3N_4 ceramic displays favorable mechanical strength, good oxidation resistance, low thermal expansion coefficient and stable dielectric constant at high temperatures (Ref 1, 2). However, dense Si_3N_4 ceramic usually demonstrates a relatively high dielectric constant (5.6 for α-Si_3N_4 and 7.9 for β-Si_3N_4), which exceeds the requirement of the microwave apparatus and missile radomes (Ref 3). Recently, intensive attentions have been paid to the preparation of porous Si_3N_4 ceramic that is capable of generating low dielectric constant while maintaining good mechanical properties (Ref 4, 5). The mechanism of high strength lies in the tailored microstructure, in which the anisotropic growth of columnar β-Si_3N_4 grains can be controlled to form an interlocked structure that strengthens the ceramic analogous to whisker-reinforced material (Ref 6, 7).

Gel-casting is an innovative approach to the preparation of porous Si_3N_4 ceramics. The basic principle of the technique is forming a three-dimensional polymer structure through in situ polymerized organic molecules to tightly hold the ceramic powders (Ref 8). The advantages include dimensional accuracy, density uniformity, complex shaping capability and cost reduction (Ref 9). It is feasible to control the porosity as well as the properties of the ceramics by adjusting the slurry solid loading and the content of organic molecules (Ref 10, 11). The quality of the obtained ceramics, however, is largely affected by different gel-casting parameters. Omatete et al. (Ref 12) reported that the critical aspects of gel-casting process include premix solution, slurry viscosity, drying process, binder burnout and strength of dried gel-casting green body. Yu et al. (Ref 13) studied the influences of the monomer content and the ratio of monomers on the performances of the green body and the sintered porous Si_3N_4 ceramics. It is revealed that the interaction of rheological behavior of the slurry, the polymerization process of the monomers and the controlling of defects in the green body were of crucial importance for the preparation of porous Si_3N_4 ceramics (Ref 14). For instance, the pH value largely determines the viscosity of ceramic slurry and is essential for preparing slurry with a high solid loading. Besides, humidity and temperature should also be carefully controlled during the drying stage in order to avoid uneven distribution of internal stress within the green body (Ref 15).

In addition to the gel-casting process, gas-pressure sintering provides an isostatic gas pressing to reduce the nonuniform shrinkage and warp of the porous Si_3N_4 ceramics during high-temperature sintering (Ref 16). The gas-pressure sintering has been successfully applied to fabricate high-quality arbitrary Si_3N_4 ceramic radome (porosity ~ 60%) and other porous wave-transparent ceramics (Ref 17, 18). We prepared porous Si_3N_4 (porosity 36.4-57.6%) with different solid loading by combining gel-casting and gas-pressure sintering process (Ref 19). To obtain high-performance porous Si_3N_4 ceramics, oxides of the rare earths (RE) and Group III elements are usually added as sintering additives (Ref 20). Those oxides additives are designed to generate intergranular liquid phase at high temperatures that would promote the rearrangement of the grains as well as the phase transition from spherical α-Si_3N_4 to columnar β-Si_3N_4 through a dissolution and re-precipitation process (Ref 21). Besides, the anisotropic growth of β-Si_3N_4 grains is found to be very sensitive to the particular additive used, which is influenced by both the adsorption behavior of

Chunrong Zou, Shaojun Guo, Xiaosong Zhou, Song Li, and **Tongsheng Shen**, Advanced Interdisciplinary Technology Research Center, National Innovation Institute of Defense Technology, Beijing 100071, China; and **Chunlei Yan**, Rocket Force University of Engineering, Xi'an 710025, China. Contact e-mails: crzou_aitrc@163.com and tongshengshen@163.com.

rare earth (RE) elements at grain surfaces and the viscosity of the intergranular phases (Ref 22, 23).

It is noticed that while a number of independent studies have been carried out on the different rheological behaviors of ceramic slurry, and the effects of concentration of monomer on gelation quality, the gel-casting parameters usually differ from different Si_3N_4 powders and oxide additives. The present study, however, is dedicated to prepare high-performance porous Si_3N_4 ceramics with Y_2O_3 and Al_2O_3 additives through an optimized gel-casting and gas-pressure sintering process. The parameters of gel-casting process for obtaining a high solid loading of 46.5vol.% were firstly optimized, and the effects of Y_2O_3: Al_2O_3 ratio on the density, β-Si_3N_4 phase content, mechanical and dielectric properties of the Si_3N_4 ceramics were then presented.

2. Experimental Procedures

2.1 Gel-Casting and Gas-Pressure Sintering

Aqueous gel-casting of Si_3N_4 was carried out using acrylamide (AM) and *N*,*N*′-methylenebisacrylamide (MBAM) as monomers and cross-linker, respectively. Ammonium persulfate (APS) was used to initiate the polymerization reactions. α-Si_3N_4 (produced by Tsinghua Unisp Lendor High Technology Ceramics Co., Beijing, China with an average particle size of $\sim$ 1.0 μm and $\alpha/(\alpha+\beta) \geq 92\%$)was used as raw powders, and Al_2O_3 (mean particle size, 0.3 μm) and Y_2O_3 (mean particle size, 0.2 μm) powders were selected as sintering additives.

The schematic procedure of gel-casting of porous Si_3N_4 perform is illustrated in Fig. 1. Firstly, the organic monomers and cross-linker were dissolved in water to form the premix solution. The amount of the organics was fixed as 5 wt.% of the ceramic powder used. Then the ceramic powders consisting 92 wt.% Si_3N_4 and 8 wt.% sintering additives (with different Y_2O_3: Al_2O_3 ratio) were added into the premix solution. To keep a high fluidity, the ceramic powders were gradually added while controlling the pH value of the slurry at 10.3-11.0 using tetramethylammonium hydroxide (TMAH) as adjuster. A high solid loading of 46.5 vol.% was achieved, and the slurry was then milled for 24 h to break down agglomerates. Secondly, after ball milling, the slurry was transferred to a modified stirring container where the APS initiator could be slowly dropped in under vacuuming condition. The degassing process is essential to eliminate the bubbles generated within the slurry. Afterward, the slurry was cast into glass molds and consolidated at 80 °C for 40 min to form gel-preforms. A typical size of the gel-preform is 60 mm (length) × 45 mm (width) × 5 mm (height). Thirdly, the gel-preforms were demolded and dried at 60 °C with a constant humidity of 50% to avoid cracking and nonuniform shrinkage. After drying, the organics contained were removed by burning out at 600 °C for 1 h in air using a heating rate of 1 °C/min. Thus, the porous Si_3N_4 preforms were obtained. Finally, the porous Si_3N_4 preforms were gas-pressure sintered at 1700 °C for 1 h with a heating rate of 10 °C/min followed by natural cooling, the pressure of the gas was maintained at 0.6 MPa during the whole sintering process. We have tried to fabricate porous Si_3N_4 ceramics in which the columnar β-Si_3N_4 grains were selectively grown by applying a specific sintering temperature of 1700 °C.

2.2 Materials Characterization

The bulk density and open porosity of the porous Si_3N_4 ceramics were measured by the Archimedes method using distilled water as medium. Crystalline phases were identified by x-ray diffraction (XRD, D8 Advance, Bruker Corp., Germany) using Ni-filtered Cu-Ka radiation. Microstructure of the ceramics was examined by scanning electron microscope (SEM, FEI Sirion 200, Holland) and transparent electron microscope (TEM/HRTEM, JEM-2010, JEOL, Japan). The room temperature bending strength of the ceramics was measured by three-point loading test (WDW-100, Changchun Research Institute of Testing Machines, Jilin, China) for at least seven specimens with a typical size of 35 mm (length) × 4 mm (width) × 3 mm (height), a span of 30 mm and a cross-head velocity of 0.5 mm/min. The room temperature dielectric constant and loss tangent of the ceramics were measured by high-Q cavity resonance method at 12.6 GHz using a vector network analyzer (AgilentN5245A, America).

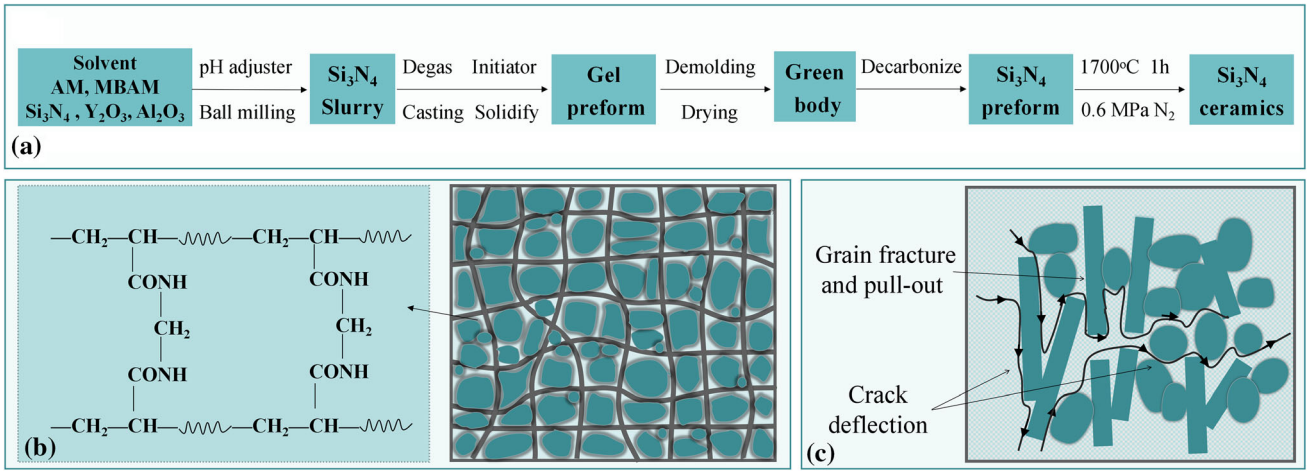

Fig. 1 (a) Schematic diagram of gel-casting process and gas pressure sintering for porous Si_3N_4 ceramics; (b) Schematic diagram of gelled preform and polymer structure; (c) Schematic diagram of different fracture modes and crack propagation within the porous Si_3N_4 ceramics

3. Results and Discussion

3.1 Optimization of Gel-Casting Parameters

The optimization of the gel-casting parameters include the pH value of Si_3N_4 slurry, degas procedure, AM: MBAM ratio, drying condition and decarbonize process. Firstly, it is essential to prepare a highly concentrated ceramic slurry with a low viscosity. The dispersion characteristic of the ceramic slurry is closely related to the surface chemistry that determined by van der Waals dispersion force and electrostatic force. The latter refers to the diffuse electric double layer between the particle surface and surrounding solution, whose charge distribution (the number of adsorbed H^+ or OH^- ions on the particle surface) is greatly influenced by pH value (Ref 12, 13). Figure 2 shows the effect of pH value on the viscosity of the Si_3N_4 slurry with a solid loading of 46.5 vol.%. The slurry viscosity was as high as 9650 mPa·s when the pH value was 9, which declined rapidly to below 130 mpa as the pH was increased to 10.3-11.0. It is indicated that when the pH value was less than 10, the electrostatic force between particles was relatively small, and the particles tended to aggregate under the driving of Van der Waals force, leading to a very high viscosity of the Si_3N_4 slurry. In the pH value range of 10.3-11.0, however, the agglomeration of the particles became significantly reduced as the electrostatic force was increased, and the viscosity of Si_3N_4 slurry quickly decreased. The low viscosity is beneficial for the composition uniformity and the casting feasibility of the Si_3N_4 slurry.

Degassing is another critical procedure for the casting of the slurry. During the milling process, air bubbles are introduced into the Si_3N_4 slurry and will yield pores in the consolidated green bodies if not excluded. Besides, monomers AM will react with pH adjuster TMAH and discharge NH_3 gas according to the following reaction:

$$C_2H_3CONH_2 + OH^- = C_2H_3COO^- + NH_3(g) \qquad \text{(Eq 1)}$$

The degree of the reactivity is low at room temperature, while the NH_3 gas is dissolved in the suspensions owing to its high solubility. However, this reaction becomes strong, and the solubility of NH_3 decreases greatly at the gel consolidation temperature of 70 °C. Therefore, degassing must be carried out

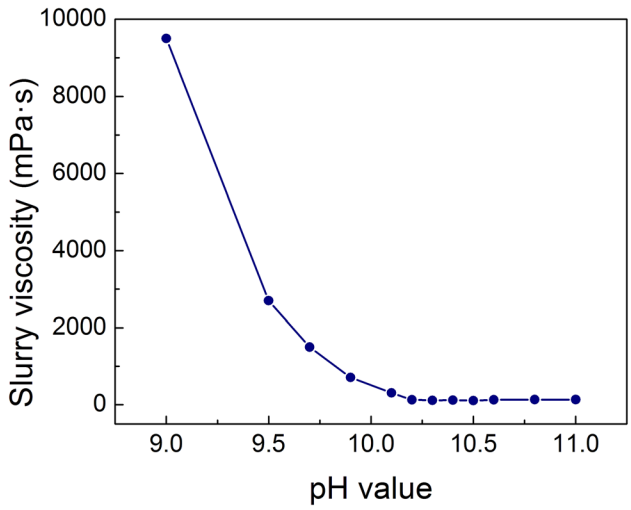

Fig. 2 Effect of pH value on the viscosity of the ceramic slurry

before casting slurry. In the present study, vacuum degassing method was applied to exclude the gases, and the vacuum was maintained at around 1×10^3 Pa. The slurry was degassed in advance for 0.5 h to remove the air bubbles and the dissolved NH_3 gas, and then kept vacuuming when adding the APS initiator. Figure 3 shows the different morphology of the sintered ceramics with and without degassing before casting. It is clear that there are more and larger pores in the ceramic without degassing procedure than that of the degassed one. Although it is difficult to completely eliminate the gasses within the slurry due to the high solubility of NH_3 gas in water, the uniform microstructure could contribute to improving the mechanical performance of the ceramic.

After the casting of the Si_3N_4 slurry, the gelation and consolidation were employed at a constant temperature of 70 °C. The gelation of the Si_3N_4 slurry is the irreversible in situ polymerization process of the monomer AM and the cross-linker MBAM under the initiation of APS. The resulted polymer network will trap and hold the ceramic particles together, as illustrated in Fig. 1(b). In specific, when subjected to the heated environment, the APS initiator will generate two free radicals and causes addition polymerization of AM monomers to form long-chain molecules; meanwhile MBAM consists two carbon–carbon double bonds that will bridge the AM chains to form a network structure, in which the ceramic particles are fixed and shaped as a whole preform. Obviously, the quality of the preform is largely related to the polymer rigidity determined by the different AM: MBAM ratios. Figure 4 shows the effect of AM: MBAM ratio on the polymer rigidity in terms of bending strength of the green body. As the AM: MBAM ratio increased from 4 to 32, the bending strength of the green body increased at first, reached its maximum value and then declined continuously. The value of 22.2 MPa was achieved with an optimal ratio of 12.

After removal from mold, the gel preform usually contains about one-fourth of its mass as moisture, which need to be removed by drying. The drying process, however, should be carefully controlled under suitable humidity and temperature so as to avoid nonuniform body shrinkage and warp. Figure 5 shows the typical mass change of gel preform with drying time at a humidity of 50% and a temperature of 60 °C for current study. The removal of water solvent can be divided into two stages (Ref 24). The first stage is the discharge of free water that gradually diffuses and migrates to the surface; and the second stage is the slow removal of water molecules adsorbed on the ceramic particles and within the polymer network. It can be seen that the mass of the gel-preform became steady after drying for 48 h, which indicates the effectiveness of the adapted humidity and temperature in providing a steady water migrating gradient for the free water.

In addition, there are many organics introduced in the precession of gel-casting, so it is necessary to remove the adverse effect of residual carbon of organics on the dielectric properties by slowly burning out the organics in air before gas pressure sintering. The thermo-gravimetric analysis (TG) was applied to characterize the mass loss of the Si_3N_4 green body, and the result is shown in Fig. 6. Clearly, there exists a fast weight loss between 200 and 500 °C, which corresponds to the evaporation of residual water and the decomposition of the organics. To avoid sample expansion and crack, the heat rate should be slow enough within this temperature range. Therefore, the adopted carbon removal process is heating the green body to 600 °C in air with a heating rate of 1 °C/min, holding

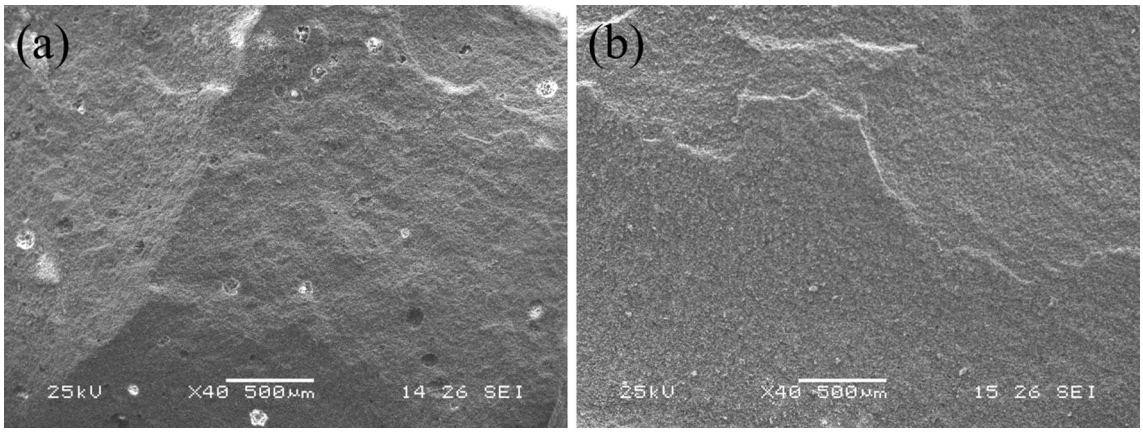

Fig. 3 Typical morphology of the sintered ceramics with and without degassing procedure

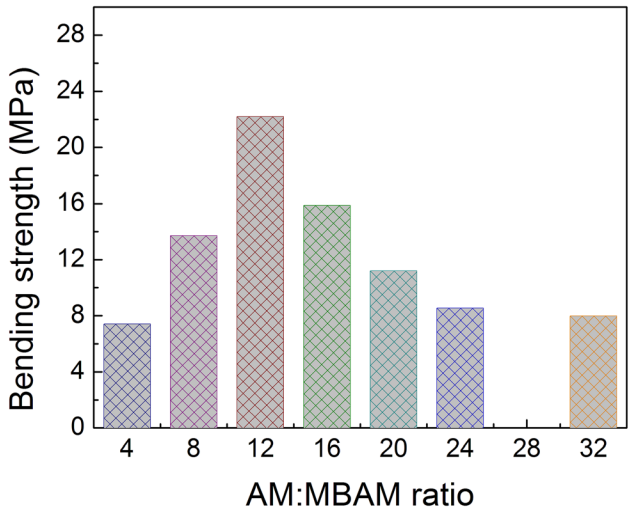

Fig. 4 Effect of AM: MBAM ratio on the bending strength of the green body

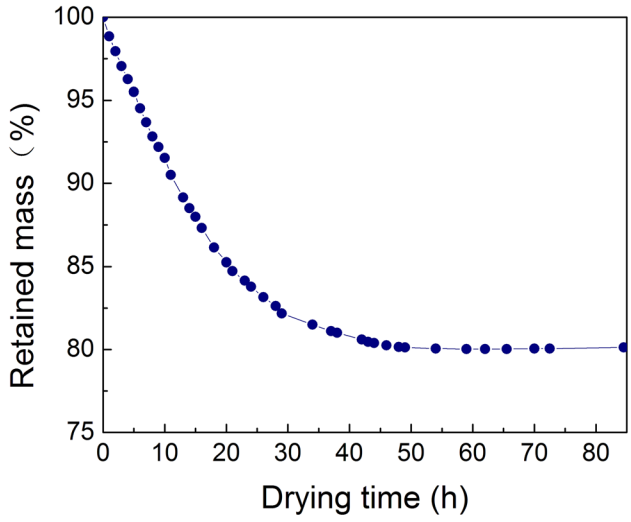

Fig. 5 Mass change of gel preform with different drying time

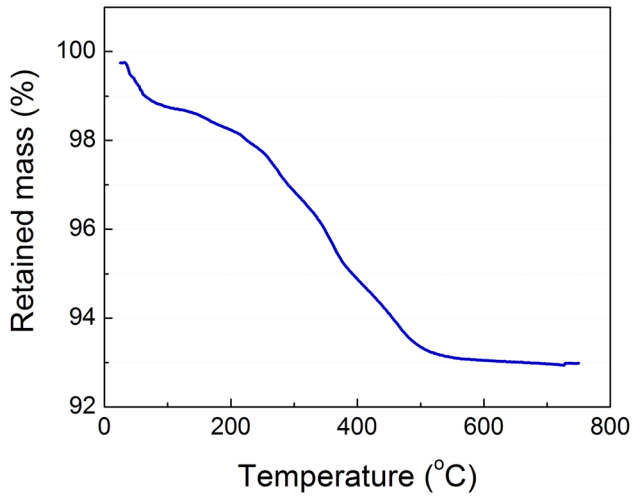

Fig. 6 Typical thermo-gravimetric curve of the Si_3N_4 green body

at 600 °C for 1 h and then cooling down with the furnace. This procession is effective for the organics removal of bulk samples in the present study in spite of the slower oxygen diffusion inside bulk samples, since the measured mass loss of the bulk samples after decarburization agrees well with the mass of organics added.

3.2 Phase Composition and Microstructure

Table 1 lists the density, open porosity, body shrinkage and β-Si_3N_4 phase content of the porous Si_3N_4 ceramics with different Y_2O_3 and Al_2O_3 contents. As the Y_2O_3 content decreased from 6 to 1 wt.%, the body shrinkage of the ceramics increased from 23.3 to 26.1%, the open porosity decreased from 36.3 to 27.5%, while the corresponding density increased from 2.07 to 2.32 g/cm^3.

Figure 7 shows the typical fracture microstructure of the sintered ceramics. All of the ceramics were composed of different amounts of spherical α-Si_3N_4 grains, elongated β-Si_3N_4 grains and pores, while the amount of β-Si_3N_4 grains decreased as the Y_2O_3 content decreased. The interlocking structure due to the mutual overlapping of elongated β-Si_3N_4 grains were clearly observed for the ceramics with 6 and

Table 1 Density, open porosity, body shrinkage and β-Si_3N_4 phase content of the porous Si_3N_4 ceramics with different contents of Y_2O_3 and Al_2O_3 additives

Y_2O_3 content, wt.%	Al_2O_3 content, wt.%	Density, g/cm^3	Open porosity, %	Body shrinkage, %	β-Si_3N_4 phase content, %
6	2	2.07	36.3	23.3	38.9
4	4	2.15	33.6	24.0	32.4
2	6	2.26	29.1	24.5	22.1
1	7	2.32	27.5	26.1	15.0

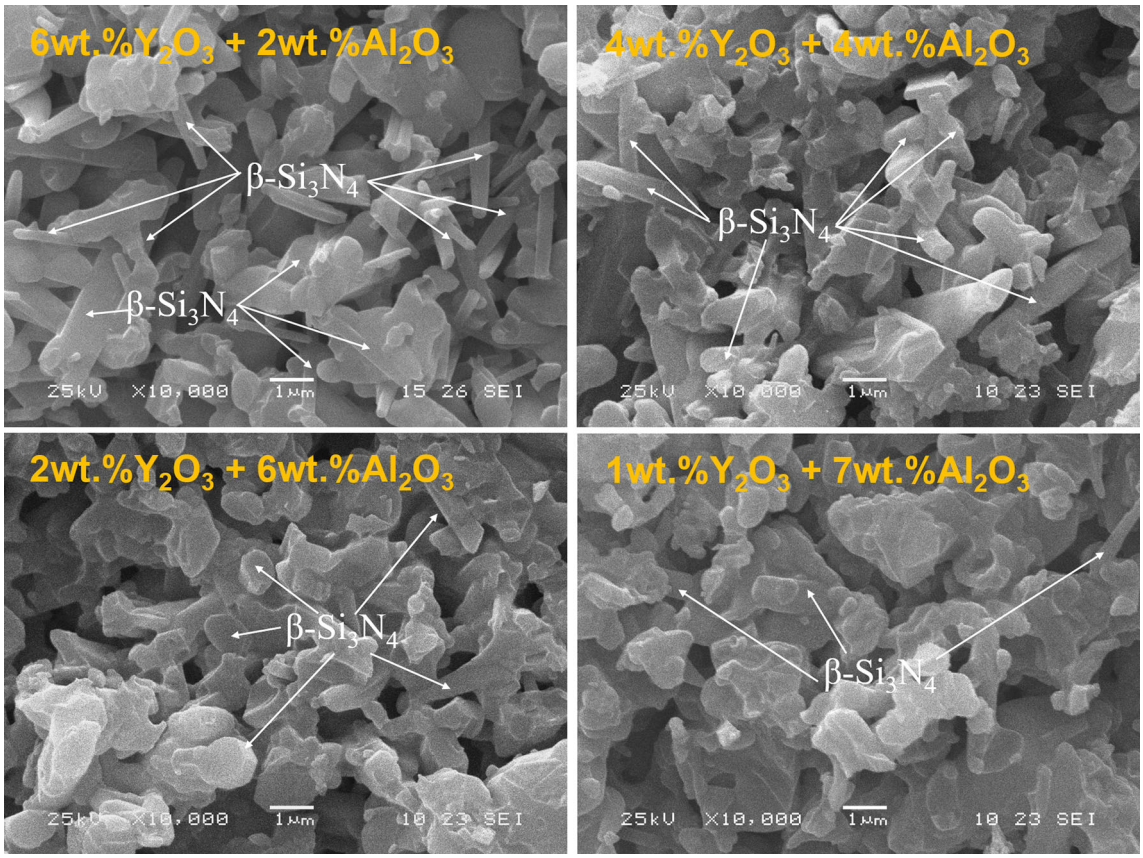

Fig. 7 Typical microstucture of the porous Si_3N_4 ceramics with different contents of Y_2O_3 and Al_2O_3 additives

4 wt.% Y_2O_3 contents. The interlocking structure of β-Si_3N_4 grains is expected to behavior superior fracture-resistant than the structure formed of α-Si_3N_4 grains. However, it became difficult to observe columnar β-Si_3N_4 for the ceramics with 2 and 1 wt.% Y_2O_3 contents. On the one hand, the β-Si_3N_4 phase was transformed from α-Si_3N_4 phase through a process of self-dissolution and resolution process. Since the β-Si_3N_4 phase content was relative low, a certain amount of the β-Si_3N_4 grains could be enfolded by the α-Si_3N_4 grains. On the other hand, the anisotropic growth of β-Si_3N_4 grains slowed down as the Y_2O_3 content decreased for, resulting in limited growth of columnar β-Si_3N_4 grains.

Figure 8 shows the phase composition of the ceramics by XRD analysis. It is shown that all of the ceramics were consisted of crystalline α-Si_3N_4 and β-Si_3N_4 grains without any other crystalline phase. The contents of β-Si_3N_4 phase (wt.%) were further determined using the peak intensities of the diffraction diagrams by formula (2) (Ref 25).

$$R_\beta = \frac{I_{\beta(101)} + I_{\beta(210)}}{I_{\beta(101)} + I_{\beta(210)} + I_{\alpha(210)} + I_{\alpha(102)}} \quad \text{(Eq 2)}$$

It is revealed that the phase content of β-Si_3N_4 grains decreased continuously from 38.9 to 15.0% as the Y_2O_3 content decreased from 6 to 1 wt.%, which is consistent with the microstructure analysis. Besides, since there was no crystalline phase containing Y and Al elements detected by the XRD analysis, an amorphous Y-Al–Si–N-O phase was expected to form between the Si_3N_4 grains given the addition of the oxide additive as well as the possibly existence of a small amount of SiO_2 due to the oxidation of Si_3N_4.

Generally, rare-earth and group III oxide additives are introduced to generate inter-granular liquid phase at high temperatures to promote the grain rearrangement and the phase transition from spherical α-Si_3N_4 to columnar β-Si_3N_4 through a dissolution and re-precipitation process (Ref 21). In the present study, the variation of Y_2O_3: Al_2O_3 ratio largely affects

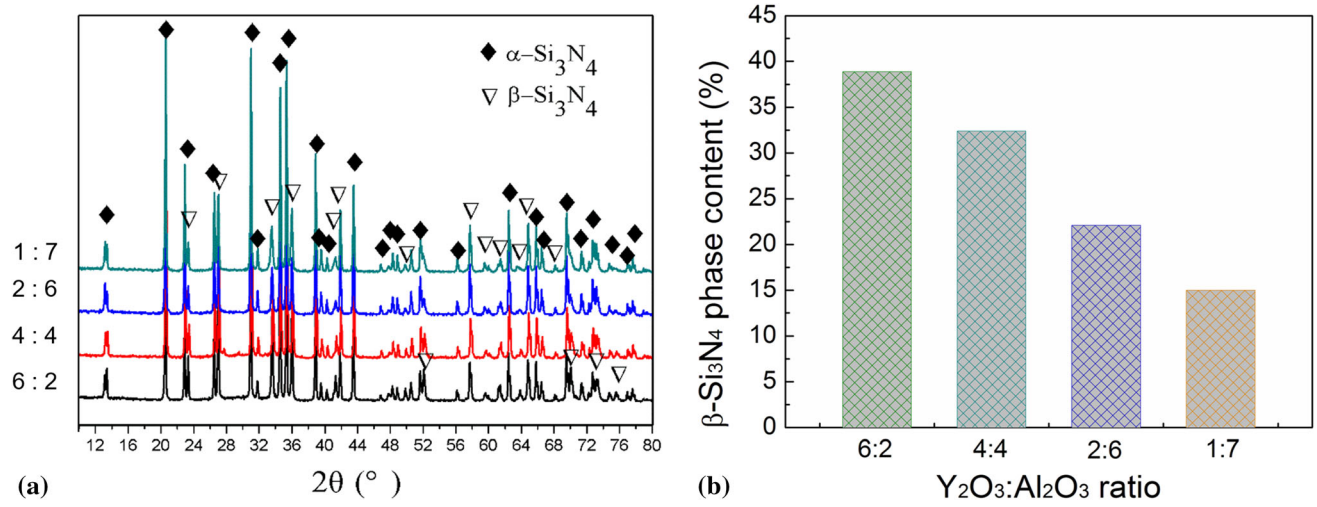

Fig. 8 (a) XRD patterns and (b) the calculated β-Si_3N_4 phase contents of the porous Si_3N_4 ceramics with different contents of Y_2O_3 and Al_2O_3 additives

Table 2 Mechanical and dielectric properties of the porous Si_3N_4 ceramics with different contents of Y_2O_3 and Al_2O_3 additives

Y_2O_3 content, wt.%	Al_2O_3 content, wt.%	Bending strength, MPa	Elastic modulus, GPa	Dielectric constant	Loss tangent
	2	205.2 ± 13.2	77.0 ± 3.9	3.46	0.0065
4	4	227.6 ± 10.3	80.4 ± 4.5	3.53	0.0063
2	6	218.4 ± 11.7	70.8 ± 4.1	3.68	0.0055
1	7	210.8 ± 12.4	63.1 ± 4.3	3.70	0.0060

the open porosity and β-Si_3N_4 content of the ceramics. Both of the open porosity and β-Si_3N_4 content decrease as the Y_2O_3: Al_2O_3 ratio decreases. The differences are mainly resulted from the different liquid viscosity and the rare-earth element sensitive anisotropic growth of β-Si_3N_4 grains. On the one hand, a certain amount of liquid is necessary for grain rearrangement and phase transformation, while the viscosity of liquid Y-Al–Si–N-O phase decreases as the Al_2O_3 content decreases, leading to accelerated grain rearrangement and lower porosity (Ref 26, 27). On the other hand, the increase of Y_2O_3 content benefits the anisotropic growth of β-Si_3N_4 grains. It is revealed that the anisotropic grain growth originates from the site competition between RE and Si for bonding at β-Si_3N_4 interfaces and within the liquid glass. Yttrium tends to segregate to the prism planes of the embedded β-Si_3N_4 grains impedes the attachment of Si-based silicon nitride growth units, and the extent of this limitation leads to the grain growth anisotropy (Ref 28, 29). Besides, the anisotropic growth of β-Si_3N_4 grains and the resulted interlocking structure would in turn interfere with densification.

3.3 Mechanical and Dielectric Properties

Table 2 summarizes the mechanical and dielectric properties of the porous Si_3N_4 ceramics with different Y_2O_3 and Al_2O_3 contents. As the Y_2O_3 content decreased from 6 to 1 wt.%, both the bending strength and elastic modulus of the ceramics undergone increasing firstly then declined continuously, and the maximum values of 227.6 MPa and 80.4 GPa were reached for a Y_2O_3: Al_2O_3 ratio of 1:1. Meanwhile, the ε value increased monotonically from 3.46 to 3.70, while the tan δ was relatively stable below 0.007.

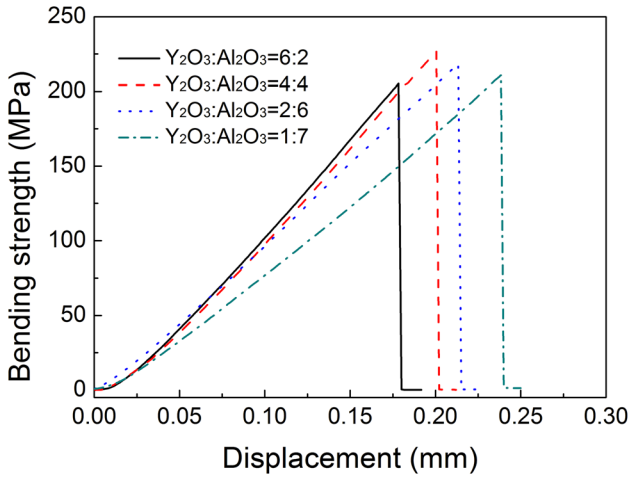

Fig. 9 Typical bending strength to displacement curves of the ceramics with different contents of Y_2O_3 and Al_2O_3 additives

Figure 9 shows the typical bending strength to displacement curves of the sintered ceramics. The ceramics displayed typical brittle fracture behaviors. Usually, it is difficult to decide whether the value of the open porosity, the shape of the pores, the higher β to α ratio, the aspect ratio of β grains or any other

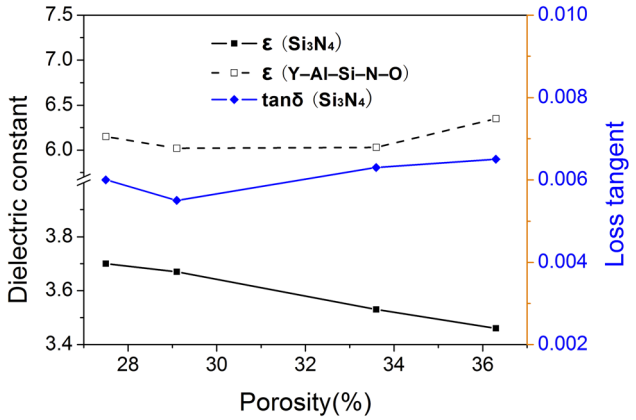

Fig. 10 Dielectric constant and loss tangent of the porous Si_3N_4 ceramics as a function of porosity

parameters have a greater effect on the mechanical properties in a porous ceramic. However, it is recognized that the bending strength of ceramics inevitably decreases with increasing porosity. Besides, it is observed that the Si_3N_4 ceramics with 6 and 1 wt.% Y_2O_3 additives displayed comparative bending strengths while the former demonstrated both higher porosity and β-Si_3N_4 phase content, which indicates that the elongated β-Si_3N_4 grains played a positive role in improving the mechanical properties (Ref 30). As addressed by Kawai et al. (Ref 25), the bending strength of porous Si_3N_4 ceramics was dominated by both the porosity and the elongated β-Si_3N_4 grain growth. Although the increasing porosity was detrimental to the flexural strength, the unique interlocking microstructure of elongated β-Si_3N_4 grains contributed to the improvement of ceramic strength by means of β-Si_3N_4 grains de-bonding and pulling out. As illustrated in Fig. 1(c), the main fracture behaviors of α-Si_3N_4 grains are de-bonding and crack deflection, while the β-Si_3N_4 grains may also fracture in terms of elongated grain bridge, rupture and pull out that are much higher energy consumption.

Besides the mechanical properties, good dielectric property is also necessary for wave transparent materials. It requires low dielectric constant ($\varepsilon < 4$) and loss tangent value (tan $\delta < 0.01$) (Ref 31). In Fig. 10, the dielectric constant and loss tangent of the Si_3N_4 ceramics are illustrated in terms of different porosities. As the porosity decreased from 36.3 to 27.5%, the ε value increased monotonically from 3.46 to 3.70, while the tan δ was relatively stable below 0.007. The dielectric values of the porous ceramics can be recognized as quite stable for practical wave-transparent application.

Besides, the dielectric constant of the amorphous Y-Al–Si–N-O phase can be calculated according to Lichtenecker mixing law as described in formula (3) (Ref 32).

$$\ln \varepsilon = V_\alpha \ln \varepsilon_\alpha + V_\beta \ln \varepsilon_\beta + V_{\text{air}} \ln \varepsilon_{\text{air}} + V_{\text{Y-Al-Si-N-O}} \ln \varepsilon_{\text{Y-Al-Si-N-O}} \quad \text{(Eq 3)}$$

where ε_i and V_i ($i = \alpha - Si_3N_4$, β-Si_3N_4, air, Y-Al–Si–N-O) stand for the dielectric constant and volume fraction of each phase, respectively. The dielectric constants of different phase are taken as α-Si_3N_4 ($\varepsilon = 5.6$), β-Si_3N_4 ($\varepsilon = 7.9$) and air ($\varepsilon = 1$). Therefore, the calculated dielectric constant of the amorphous Y-Al–Si–N-O phase fluctuates in the range of 6.02-6.36, and the average value is 6.14.

In the future, it would be worth exploring the optimization of sintering temperatures as well as the high temperature properties of the Si_3N_4 ceramics.

4. Conclusions

Porous Si_3N_4 ceramics were prepared by optimized gel-casting process and gas pressure sintering, and the effects of Y_2O_3: Al_2O_3 ratio on the microstructure and properties of the ceramics were investigated. The conclusions are drawn as follows:

(1) A high slurry solid loading of 46.5 vol.% was achieved using the optimized gel-casting parameters, including an optimal slurry pH value between 10.3 and 11.0, an AM: MBAM ratio of 12, and a drying time beyond 48 h at 60 °C and 50% humidity.
(2) As the Y_2O_3 content decreased from 6 to 1 wt.%, the open porosity of the sintered ceramics decreased from 36.3 to 27.5%, and the phase content of β-Si_3N_4 grains decreased from 38.9 to 15.0%. Increasing Y_2O_3 content tended to promote the phase transformation and anisotropic growth of β-Si_3N_4 grains.
(3) The elongated β-Si_3N_4 grains was beneficial for the mechanical properties of the ceramics and the ceramic with 4 wt.% of Y_2O_3 and 4 wt.% of Al_2O_3 additives displayed high bending strength and elastic modulus of 227.6 MPa and 80.4 GPa, respectively. The Si_3N_4 ceramics also exhibited low dielectric constant and loss tangent of 3.46-3.70 and 0.0055-0.0065.

Acknowledgments

We gratefully acknowledged the financial support from the National Natural Science Foundation of China (Grant No. 51802348) and Shanxi Provincial Natural Science Foundation of China (Grant No. 2018JQ5111).

References

1. F.L. Riley, Silicon Nitride and Related Materials, *J. Am. Ceram. Soc.*, 2000, **83**(2), p 245–265
2. H. Klemm, Silicon Nitride for High-Temperature Applications, *J. Am. Ceram. Soc.*, 2010, **93**(6), p 1501–1522
3. E.I. Suzdaltsev, Radio-Transparent Ceramics: Yesterday, Today, Tomorrow, *Refract. Indust. Ceram.*, 2015, **55**, p 377–390
4. T. Ohji, Microstructural Design and Mechanical Properties of Porous Silicon Nitride Ceramics, *Mater. Sci. Eng., A*, 2008, **498**(1), p 5–11
5. S. Yin, L. Pan, L. Guo, Y. Liu, Y. Feng, T. Qiu, and J. Yang, Fabrication and Properties of Porous Si_3N_4 Ceramics by Aqueous Gel-Casting Using Low-Toxic DMAA Gelling Agent, *Ceram. Int.*, 2018, **44**(7), p 7569–7579
6. Z. Shen, Z. Zhao, H. Peng, and M. Nygren, Formation of Tough Interlocking Microstructures in Silicon Nitride Ceramics by Dynamic Ripening, *Nature*, 2002, **417**(6886), p 266–269
7. S. Yin, L. Pan, Y. Liu, Y. Wang, T. Qiu, and J. Yang, Effect of β-Si_3N_4 Seeds on Microstructure and Properties of Porous Si_3N_4 Ceramics Prepared by Gel-Casting Using DMAA System, *Ceram. Int.*, 2020, **46**(4), p 4924–4932

8. L. Montanaro, B. Coppola, P. Palmero, and J.M. Tulliani, A Review on Aqueous Gel-Casting: A Versatile and Low-Toxic Technique to Shape Ceramics, *Ceram. Int.*, 2019, **45**(7), p 9653–9673
9. A.C. Young, O.O. Omatete, M.A. Janney, and P.A. Menchhofer, Gel-Casting of Alumina, *J. Am. Ceram. Soc.*, 1991, **74**(3), p 612–618
10. M.H. Bocanegra-Bernal and B. Matovic, Dense and Near-Net-Shape Fabrication of Si_3N_4 Ceramics, *Mater. Sci. Eng., A*, 2009, **500**, p 130–149
11. J. Wu, X. Zhang, and J. Yang, Novel Porous Si_3N_4 Ceramics Prepared by Aqueous Gel-Casting Using Si_3N_4 Poly-Hollow Microspheres as Pore-Forming Agent, *J. Eur. Ceram. Soc.*, 2014, **34**(5), p 1089–1096
12. O. Omatete, M.A. Janney, and S.D. Nunn, Gelcasting from Laboratory Development Toward Industrial Production, *J. Eur. Ceram. Soc.*, 1997, **17**, p 407–413
13. J.L. Yu, H. Wang, H. Zeng, and J. Zhang, Effect of Monomer Content on Physical Properties of Silicon Nitride Ceramic Green Body Prepared by Gel-Casting, *Ceram. Int.*, 2009, **35**(3), p 1039–1044
14. J. Yu, J. Yang, and Y. Huang, The Transformation Mechanism from Suspension to Green Body and the Development of Colloidal Forming, *Ceram. Int.*, 2011, **37**, p 1435–1451
15. W. Zeng, X. Gan, Z. Li, and K. Zhou, The Preparation of Silicon Nitride Ceramics by Gel-Casting and Pressureless Sintering, *Ceram. Int.*, 2016, **42**(10), p 11593–11597
16. S. Hwang, P.F. Becher, and H. Lin, Desintering Process in the Gas-Pressure Sintering of Silicon Nitride, *J. Am. Ceram. Soc.*, 2005, **80**(2), p 329–335
17. L. Yong, F. Chen, L. Ling, W. Zhang, H. Yu, Y. Shan, Q. Shen, and H. Jiang, Gas Pressure Sintering of Arbitrary Porous Silicon Nitride Ceramics with High Mechanical Strength, *J. Am. Ceram. Soc.*, 2010, **93**(6), p 1565–1568
18. J.F. Yang, Z.Y. Deng, and T. Ohji, Fabrication and Characterization of Porous Silicon Nitride Ceramics Using Yb_2O_3 as Sintering Additive, *J. Eur. Ceram. Soc.*, 2003, **23**(2), p 371–378
19. C. Zou, C. Zhang, B. Li, S. Wang, and F. Cao, Microstructure and Properties of Porous Silicon Nitride Ceramics Prepared by Gel-Casting and Gas Pressure Sintering, *Mater. Des.*, 2013, **44**, p 114–118
20. S. Hampshire and M.J. Pomeroy, Grain Boundary Glasses in Silicon Nitride: A Review of Chemistry, Properties and Crystallisation, *J. Eur. Ceram. Soc.*, 2012, **32**(9), p 1925–1932
21. X. Tong, J. Li, X. Yang, H. Lin, G. Guo, and M. He, Mechanical Property and Oxidation Behavior of Self-reinforced Si_3N_4 Doped with Re_2O_3 (Re = Yb, Lu), *J. Am. Ceram. Soc.*, 2006, **89**(5), p 1730–1732
22. N. Shibata, S.J. Pennycook, T.R. Gosnell, G.S. Painter, W.A. Shelton, and P.F. Becher, Observation of Rare-Earth Segregation in Silicon Nitride Ceramics at Subnanometre Dimensions, *Nature*, 2004, **428**(6984), p 730–733
23. P.F. Becher, N. Shibata, and G.S. Painter, Observations on the Influence of Secondary Me Oxide Additives (Me = Si, Al, Mg) on the Microstructural Evolution and Mechanical Behavior of Silicon Nitride Ceramics Containing RE_2O_3 (RE = La, Gd, Lu), *J. Am. Ceram. Soc.*, 2010, **93**(2), p 570–580
24. J. Yang, J. Yu, and Y. Huang, Recent Developments in Gel-Casting of Ceramics, *J. Eur. Ceram. Soc.*, 2011, **31**(14), p 2569–2591
25. C. Kawai and A. Yamakawa, Effect of Porosity and Microstructure on the Strength of Si_3N_4: Designed Microstructure for High Strength, High Thermal Shock Resistance, and Facile Machining, *J. Am. Ceram. Soc.*, 1997, **80**, p 2705–2708
26. S. Hampshire and K.H. Jack, The Kinetics of Densitification and Phase Transformation in Nitrogen Ceramics, *Proc. Brit. Soc.*, 1981, **31**, p 37–39
27. M. Kramer, D. Wittmuss, and H. Kuppers, Relations Between Crystal Structure and Growth Morphology of β-Si_3N_4, *J. Cryst. Growth*, 1994, **140**, p 157–166
28. G.S. Painter, P.F. Becher, W.A. Shelton, R.L. Satet, and M.J. Hoffmann, Differential Binding Model: Effects of Rare-Earths on β-Si_3N_4 Grain Growth and Microstructure, *Phys. Rev. B*, 2004, **70**(144108), p 1–4
29. O.A. Lukianova, V.V. Krasilnikov, A.A. Parkhomenko, and V.V. Sirota, Microstructure and Phase Composition of Cold Isostatically Pressed and Pressureless Sintered Silicon Nitride, *Nanoscale Res. Lett.*, 2016, **11**(1), p 148
30. D. Li, B. Li, X. Yang, S. Gao, and Y. Zheng, Fabrication and Properties of In Situ Silicon Nitride Nanowires Reinforced Porous Silicon Nitride (SNNWs/SN) Composites, *J. Eur. Ceram. Soc.*, 2018, **38**(6), p 2671–2675
31. T. Zhang, S. Sun, J. Cai, L. Wang, J. Zhang, R. Meng, X. Huang, G. Wen, L. Huang, L. Xia, and B. Zhong, A New Precursor to Lightweight Porous Si-Al-O-B Ceramics with Enhanced Microwave Transmissivity, *Ceram. Int.*, 2020, **46**(2), p 1974–1981
32. M.B. Othman, M.R. Ramli, L.Y. Tyng, Z. Ahmad, and H.M. Akil, Dielectric Constant and Refractive Index of Poly (Siloxane–Imide) Block Copolymer, *Mater. Des.*, 2011, **32**(6), p 3173–3182